Featured in Physics

## Optical Guiding in Meter-Scale Plasma Waveguides

B. Miao<sup>®</sup>, \*L. Feder<sup>®</sup>, \*J. E. Shrock<sup>®</sup>, A. Goffin<sup>®</sup>, and H. M. Milchberg<sup>®</sup>
Institute for Research in Electronics and Applied Physics University of Maryland, College Park, Maryland 20742, USA

(Received 26 May 2020; revised 5 July 2020; accepted 20 July 2020; published 14 August 2020)

We demonstrate a new highly tunable technique for generating meter-scale low density plasma waveguides. Such guides can enable laser-driven electron acceleration to tens of GeV in a single stage. Plasma waveguides are imprinted in hydrogen gas by optical field ionization induced by two time-separated Bessel beam pulses: The first pulse, a  $J_0$  beam, generates the core of the waveguide, while the delayed second pulse, here a  $J_8$  or  $J_{16}$  beam, generates the waveguide cladding, enabling wide control of the guide's density, depth, and mode confinement. We demonstrate guiding of intense laser pulses over hundreds of Rayleigh lengths with on-axis plasma densities as low as  $N_{e0} \sim 5 \times 10^{16}$  cm<sup>-3</sup>.

DOI: 10.1103/PhysRevLett.125.074801

Laser wakefield acceleration (LWFA) of electrons in plasmas has been widely studied in the last several decades [1,2]. While compact, high repetition rate LWFA systems can generate ~10 MeV ultrashort electron bunches [3,4] for numerous applications, high repetition rate generation of multi-GeV bunches is needed for future laser-driven accelerator modules for compact light sources [5] and high energy physics [6,7]. In order to achieve such high energy over relatively short acceleration distances, LWFA requires propagation of high intensity laser pulses over many Rayleigh lengths; some form of optical waveguiding is needed.

Two types of optical guiding in plasmas have been demonstrated: relativistic self-guiding and guiding in preformed plasma waveguides. Acceleration to multi-GeV energies, while avoiding dephasing and depletion [2,8,9], requires long laser propagation distances at low plasma densities ( $< \sim 5 \times 10^{17}$  cm<sup>-3</sup>), for which self-guiding, in the highly nonlinear bubble regime, demands at least petawatt laser powers [10]. For future high repetition rate accelerators using less laser energy, the use of preformed plasma waveguides, in the quasilinear acceleration regime, presents an attractive alternative [2,11]. Preformed guides may even have advantages for bubble-regime acceleration [12], including suppression of pulse head erosion.

The first demonstrated plasma waveguide used hydrodynamic cylindrical shock expansion of gas target plasmas driven by inverse bremsstrahlung (IB) plasma heating by a ~100 ps axicon-generated Bessel beam pulse; efficient IB heating required a minimum electron density  $>\sim 5\times 10^{18}\,\mathrm{cm}^{-3}$  [13]. Shock expansion established the required concave radial electron density profile for optical guiding: an on-axis electron density minimum  $N_{e,0}$  (the "core") surrounded by the cylindrical shock wall (the "cladding"). Later work using laser heating of atomic cluster plasmas achieved even lower density waveguides with  $N_{e,0}\sim 10^{18}\,\mathrm{cm}^{-3}$  [14]. Most recently, the

hydrodynamic shock principle was extended to gas targets driven by optical field ionization (OFI) by ultrashort pulses focused by lenses [15–17] or axicons [18]. An advantage of this type of waveguide is that the quasibound mode structure allows deleterious high order modes to radiate away [19–21].

Another approach adopted in many experiments is the electrical discharge capillary waveguide [22,23]. Here, the guiding channel is determined by the plasma temperature profile established by the heat flow from the hot center to the cold wall of the capillary. This scheme offered, as originally conceived, the advantage of not requiring a laser. Recently, however, an experiment demonstrating 8 GeV electron acceleration in a 20 cm long discharge capillary [24] required auxiliary laser heating to adequately reduce the waveguide core density. A concern with discharge capillaries is their increased heat load and material erosion at high repetition rates [25], limitations that are far less onerous for laser-generated plasma waveguides.

Laser-driven OFI waveguides relying on hydrodynamic shock expansion are limited to electron temperatures comparable to the electron ponderomotive energy in the laser field at the ionization threshold of the gas [26], limiting both the height and width of the mode-confining shock wall. At the hydrogen ionization threshold of  $\sim 10^{14}$  W/cm²,  $T_e < \sim 10$  eV for a  $\lambda = 1~\mu m$  laser, resulting in weak expansion and shallow walls with weak optical confinement [18,27]. OFI heating can be enhanced by using a gas with higher ionization potential such as helium [35], but for a fixed pulse width, the laser energy must be increased by  $> 100 \times compared$  to hydrogen.

In this Letter, we present a new approach to OFIgenerated waveguides and demonstrate high intensity optical guiding up to hundreds of Rayleigh ranges. Our approach decouples the generation of the needed electron density profile from plasma heating and does

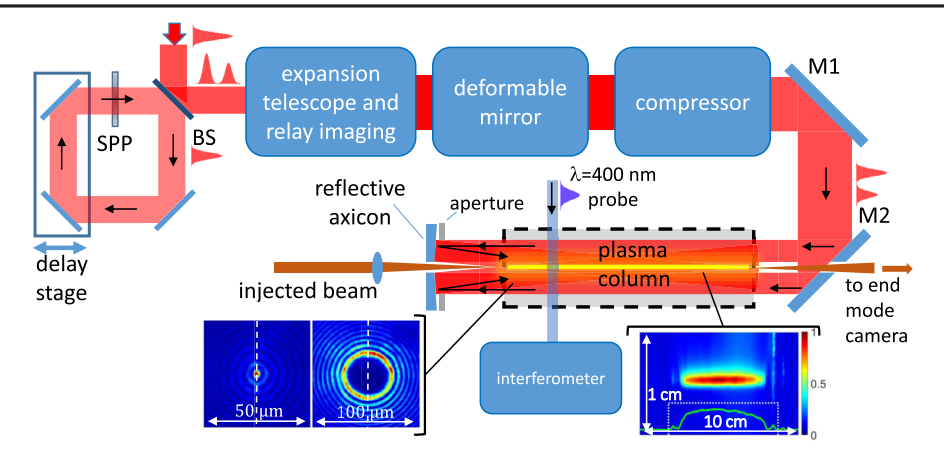


FIG. 1. Experimental setup. The ~200 ps uncompressed pulse from a Ti:Sapphire amplifier is split by a nonpolarizing beam splitter (BS). The transmitted pulse is converted to a (0,q) beam by a segmented  $q^{th}$  order spiral phase plate (SPP). After beam expansion and relay imaging, phase front correction using a deformable mirror, and recompression, the beam is focused by a reflective axicon in either backfill hydrogen gas or over a supersonic gas jet. The counterpropagating guided beam is injected into the waveguide through a hole in the axicon and imaged after guiding. Also shown frequency-doubled ( $\lambda = 400$  nm, 70 fs) interferometric probe pulse. Left bottom inset: images of  $J_0$  and  $J_{16}$  beams in focus. Right bottom inset:  $J_0$ -pulse-induced plasma fluorescence 3.5 mm above the 5 cm supersonic  $H_2$  jet.

not exclusively rely on hydrodynamic expansion. It leverages the idea that OFI can effectively imprint prescribed electron density profiles while minimally heating them. Importantly, our method enables control over both the cladding height and thickness, crucial for significantly reducing guided mode leakage losses; leakage attenuation lengths are increased to several meters from the centimeter scale of hydrodynamic OFI waveguides.

As detailed in Fig. 1, an amplified and stretched (to ~200 ps) linearly polarized  $\lambda = 800$  nm pulse from a Ti: Sapphire laser is split at an 80/20 nonpolarizing beam splitter, with 80% of the energy entering a delay ring containing a transmissive spiral phase plate to impose either a  $16\pi(q=8)$  or  $32\pi(q=16)$  azimuthal phase screw on the beam. The recombined output is a (p = 0, m = 0)Laguerre super-Gaussian pulse followed, at a delay  $\tau_d = 1-3$  ns, by a (p = 0, m = q) pulse, where p and m are radial and azimuthal mode indices. The beam is then expanded and relay imaged, phase front corrected, recompressed to 50-100 fs FWHM, and directed to a 50.8 mm diameter reflective axicon in an experimental chamber. The  $4 \times$  relay imaging conveys the plane of the spiral phase plate to the axicon. Phase front correction improves the quality of the q = 8 or q = 16 beams, employing a deformable mirror using a phase front retrieval technique developed by our group [36]. The reflective axicon forms a double-pulsed Bessel-Gauss beam, identified here using only the Bessel notation as a  $J_0$  pulse followed  $\tau_d = 1-3$  ns later by a  $J_a$ pulse. The  $J_0$  pulse forms the core of the plasma waveguide by OFI; the  $J_q$  pulse forms the cladding. Here we use a  $H_2$ backfill target (entire vacuum chamber filled) or an elongated H<sub>2</sub> gas jet.

In our experiments, the Bessel beam depth of focus, or line focus length, is  $L \approx (R - a_h)/\tan \gamma \gtrsim 15$  or 30 cm

where R = 2 cm is the radius of the outer aperture near the axicon surface,  $a_h$  is the radius of the axicon central hole,  $\gamma = 2\alpha$  is the Bessel beam ray approach angle to the optical axis, and  $\alpha = 1.5^{\circ}$  or  $3^{\circ}$  is the axicon base angle. The inner and outer edges at  $a_h$  and R set up  $\sim 1$  mm transitions of Bessel beam intensity at the extremes of the focal line, preventing excessive axial taper of the plasma there. In vacuum, the central peak radius of the  $J_0$  beam was  $r_0 =$  $2.405/k \sin \gamma = 6$  or 3  $\mu$ m, where k is the laser vacuum wave number. The initial  $J_0$  pulse fully ionizes the hydrogen gas target, creating a long, thin plasma column that expands cylindrically outward, leaving a region of low electron density near the optical axis, creating the core of the plasma waveguide. The delayed  $J_q$  pulse generates a long, cylindrical plasma shell [37–39] around the expanded column: this serves as the lower refractive index cladding. The intense pulse to be guided is focused through the axicon central hole and coupled into the waveguide.

An important first requirement is for the  $J_0$  pulse to fully ionize the hydrogen gas target to prevent ionization defocusing of the guided pulse. We found that an optical axis-averaged peak intensity of  $\sim 4 \times 10^{14} \text{ W/cm}^2$  in the  $J_0$ central maximum was sufficient to fully ionize the hydrogen gas and clamp the electron temperature along the focal line sections used in our experiments, despite the axial variation in the intensity dictated by the mapping of the beam profile to the focal line  $I(z) = I_0 z \exp[-(z/w)^n]$  $(z = r/\tan \alpha, r \ge a_h, n \approx 6)$ . Figures 2(a) and 2(b) plot cuts of  $J_0$  alone and combined  $J_0 + J_{16}$  along the white dashed plane edges in Fig. 1. These composite images were obtained by scanning a  $10 \times$  microscope objective along z. The profiles remain relatively uniform over tens of centimeters, with z variations mostly from radial variations of the input beam. Figure 2(c) shows Fig. 2(b) azimuthally

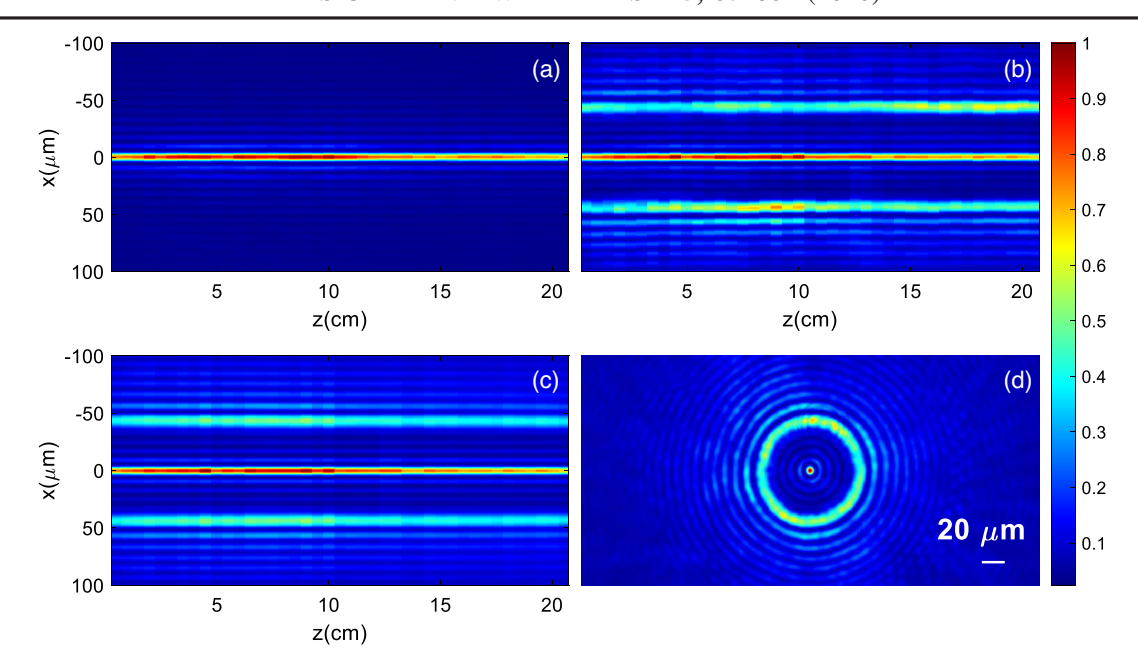


FIG. 2. (a) Optical axis scan of  $J_0$  focal spot profiles with planar cut shown in Fig. 1 inset. (b) Optical axis scan of combined  $J_0$  and  $J_{16}$  beam, with planar cut shown in Fig. 1 inset. (c) Azimuthal average of (b). (d) Combined  $J_0 + J_{16}$  beam profile.  $\gamma = 3^{\circ}$ .

averaged, and Fig. 2(d) shows a transverse cut across z of the combined beams.

After OFI by the  $J_0$  pulse, the electrons thermalize over the electron-electron collision time  $\tau_{ee} < 1$  ps, for  $N_e \sim$  $10^{18} \text{ cm}^{-3}$  and initial electron temperature  $T_{e0} < \sim 10 \text{ eV}$ , leaving a warm plasma column surrounded by cold, neutral hydrogen gas. The plasma column rapidly cools as it expands outward as a cylindrical blast expansion  $R_s(t) =$  $\xi_0(\varepsilon_0/\rho)^{1/4}t^{1/2}$ , where  $R_s$  is the radial position of the outer plasma boundary,  $\varepsilon_0$  (  $\propto T_{e0}$ ) is the laser energy deposition per unit length,  $\rho$  is the initial mass density of the hydrogen gas, and  $\xi_0$  is a dimensionless prefactor of order unity [40]. Typical plots of  $R_s(t)$  and associated density profiles are shown in Figs. 3(a) and 4(a), respectively, for peak  $J_0$ intensity 1015 W/cm2 and backfill hydrogen pressure of 50 torr. The electron temperature  $T_e$  is determined from the ion acoustic speed as  $dR_s/dt \approx c_s = (\gamma_c T_e/m_i)^{1/2}$ , where  $\gamma_c$  is the specific heat ratio and  $m_i$  is the proton mass. It is seen that, after a few nanoseconds, the expansion stagnates as the plasma cools to > 1 eV, with the central plasma density reduced by  $\sim 10 \times$  and the column expanded by  $\sim$ 3–5×. Two-color interferometry and integration of the total phase shift from the plasma column indicate that there is no recombination on this timescale. The weak  $(T_{e0})^{1/4}$ dependence of the plasma expansion ensures that moderate axial variations in Bessel beam intensity negligibly affects the local axial uniformity of the waveguide plasma, as seen in Fig 3(b).

After the  $J_0$  pulse has formed the core of the plasma waveguide, the delayed  $J_q$  pulse forms the cladding. The index q of the high order beam and its delay are chosen so that it propagates through the expanded  $J_0$  plasma column,

forming a high intensity annulus at its edge, ionizing the neutrals there. The annular plasma formed by a  $J_{16}$  pulse alone is shown in Fig. 3(c), as a function of delay after generation at t=0, and in Fig. 3(d) at t=0 as a function of  $J_{16}$  pulse energy. It is seen that the annular plasma cladding decays over  $\sim 0.5$  ns, mainly by filling in the central hole, and that the cladding height saturates at > 50 mJ.

The effect of the  $J_0$ -generated plasma on the propagation of the  $J_q$  pulse was calculated using a simulation of ultrashort pulse Bessel beam propagation including OFI and the Kerr effect (Supplemental Material [27]). Figure 4(b) shows the  $J_{16}$  pulse-generated electron density profiles with and without the  $J_0$ -generated core plasma present. The effect of the preformed core plasma on the  $J_{16}$  pulse propagation and induced OFI profile is seen to be negligible. In general, unless the core plasma density approaches the effective critical density  $N_{\rm cr,eff} = N_{\rm cr} \sin^2 \gamma \sim 0.5 - 2 \times 10^{19} \, {\rm cm}^{-3}$  experienced by oblique Bessel beam rays, it has a negligible effect on the  $J_a$ -induced ionization profile.

The two-Bessel-pulse method of plasma waveguide generation enables very wide tuning of the plasma waveguide transverse profile and its guided modes through control of the hydrogen density, the order q of the second pulse, the Bessel beam axis approach angle  $\gamma(=2\alpha)$ , the energy and pulse width of the two pulses, and the time delay between them. The plots in Figs. 4(c)-4(f) illustrate this flexibility. Here, the delay between the  $J_0$  and  $J_q$  pulses is  $\tau_d=2.4$  ns. In general, the desired guided optical mode dictates the required waveguide profile, with leaky mode or beam propagation method simulations (Supplemental Material[27]) providing the best design guidance. A good design approximation, however, recognizes the steplike

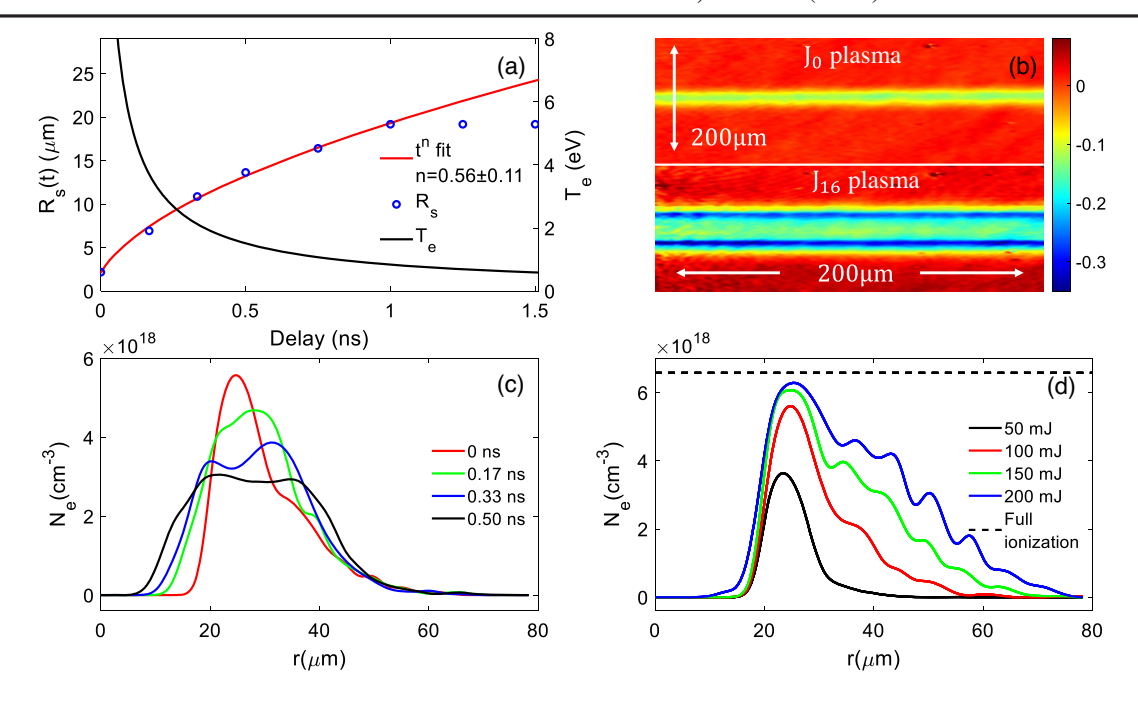


FIG. 3. (a) Radius of blast wave expansion of  $J_0$  plasma (best fit  $n = 0.56 \pm 0.11$ ) and extracted electron temperature vs time. Hydrogen backfill 50 torr. (b) Interferometric phase shift images of  $J_0$  and  $J_{16}$  plasmas 10 ps after generation. Hydrogen backfill 100 torr. (c) Time evolution of  $J_{16}$ -generated annular electron density profile. Pulse energy 100 mJ, hydrogen backfill 100 torr. The plasma pressure gradient mainly drives filling of the central hole. The radial integral of these curves (total charge) is constant to within  $\sim 5\%$ . (d) Pulse energy dependence of  $J_{16}$ -generated annular electron density profiles, with saturation for > 50 mJ. Hydrogen backfill 100 torr. The modulations at larger radius are from ionization by outer rings of the  $J_{16}$  pulse.

profiles of our two-pulse OFI waveguides: a relatively flat core and sharply rising cladding, for which the fundamental channel mode radius is given by [41]  $w_{\rm ch} \approx a(0.6484+1.619V^{-3/2}+2.879V^{-6}+\cdots)$ , where a is the core radius and the step index fiber parameter is  $V=ka(n_{\rm core}^2-n_{\rm cladding}^2)^{1/2}=a(4\pi r_e\Delta N_e)^{1/2}$ , where  $\Delta N_e=N_e^{\rm cladding}-N_e^{\rm core}$ ,  $r_e$  is the classical electron radius, and k is the laser vacuum wave number. Larger guided modes can be supported by smaller core-cladding differences  $\Delta N_e$ , which require lower hydrogen density  $N_0$  (since under OFI,  $\Delta N_e$  is roughly proportional to  $N_0$ ).

This mode scaling is illustrated in Fig. 4, where the H<sub>2</sub> density in Fig. 4(c) is chosen to be  $5 \times$  higher than in Fig. 4(d). Both experiments use a  $J_{16}$  pulse to generate the waveguide cladding, the approach angle decreasing from  $\gamma = 6^{\circ}$  in Fig. 4(c) to  $\gamma = 3^{\circ}$  in Fig. 4(d). This has the effect of widening the initial  $J_0$ -generated fully ionized core plasma and moving the cladding peak from a radial position of  $\sim 30 \ \mu m$  out to  $\sim 50 \ \mu m$ . In both cases, the core plasma remains unaffected by the second pulse, as seen by the merging of the blue and green curves toward the waveguide axis. In Fig. 4(c),  $\Delta N_e \sim 1.3 \times 10^{18} \text{ cm}^{-3}$ ,  $a \sim 20 \ \mu\text{m}$ , and  $V \sim 4.3$ , predicting  $w_{\rm ch} \sim 17 \ \mu \rm m$ , while in Fig. 4(d),  $\Delta N_e \sim 0.5 \times 10^{18} \text{ cm}^{-3}$ ,  $a \sim 40 \ \mu\text{m}$ , and  $V \sim 5.4$  give  $w_{\rm ch} \sim 32 \ \mu {\rm m}$ . We also plot the fundamental modes and their 1/e intensity attenuation lengths  $L_{1/e}$  computed using our leaky mode solver [19,27], showing good agreement with the step index values. As an example of the control available for sculpting transverse profiles, Fig. 4(e) shows use of a  $J_8$  pulse at approach angle  $\gamma=3^\circ$ . Here, the peaks of the first and second  $J_8$  rings overlap with ~50% ionized hydrogen in the expanded plasma from the  $J_0$  pulse, generating an inner cladding bump, while the third ring overlaps neutral hydrogen gas on the plasma periphery (Supplemental Material[27]), generating a higher outer cladding bump. Considering this as a step index profile to the first cladding bump (with  $\Delta N_e \sim 0.5 \times 10^{18}$  cm<sup>-3</sup>,  $a \sim 15~\mu\text{m}$ , and  $V \sim 2.0$ ), gives  $w_{\text{ch}} \sim 19~\mu\text{m}$ , in good agreement with the leaky mode solver.

We have presented results thus far for waveguides generated in  $\rm H_2$  backfill gas. For LWFA, however, distortion-free injection and guiding of high intensity pulses demands that the waveguide entrance and exit be free of neutral gas. For this purpose, we have developed a supersonic gas jet producing uniform low pressure flows. The inset to Fig. 1 shows uniform fluorescence from  $J_0$  pulse-induced OFI of a 5 cm long  $\rm H_2$  gas sheet, 3.5 mm above the nozzle orifice, where the pressure is ~30 Torr. The 15 cm long Bessel beam focus overfills the gas sheet. For jets longer than ~5 cm, the gas nozzle interferes with  $J_q$  formation in the focus; we have recently developed an optical fix for this limitation [42]. Figure 4(f) shows results from two-pulse OFI waveguide generation in the gas jet, where a steplike guide is clearly formed. Applying the step

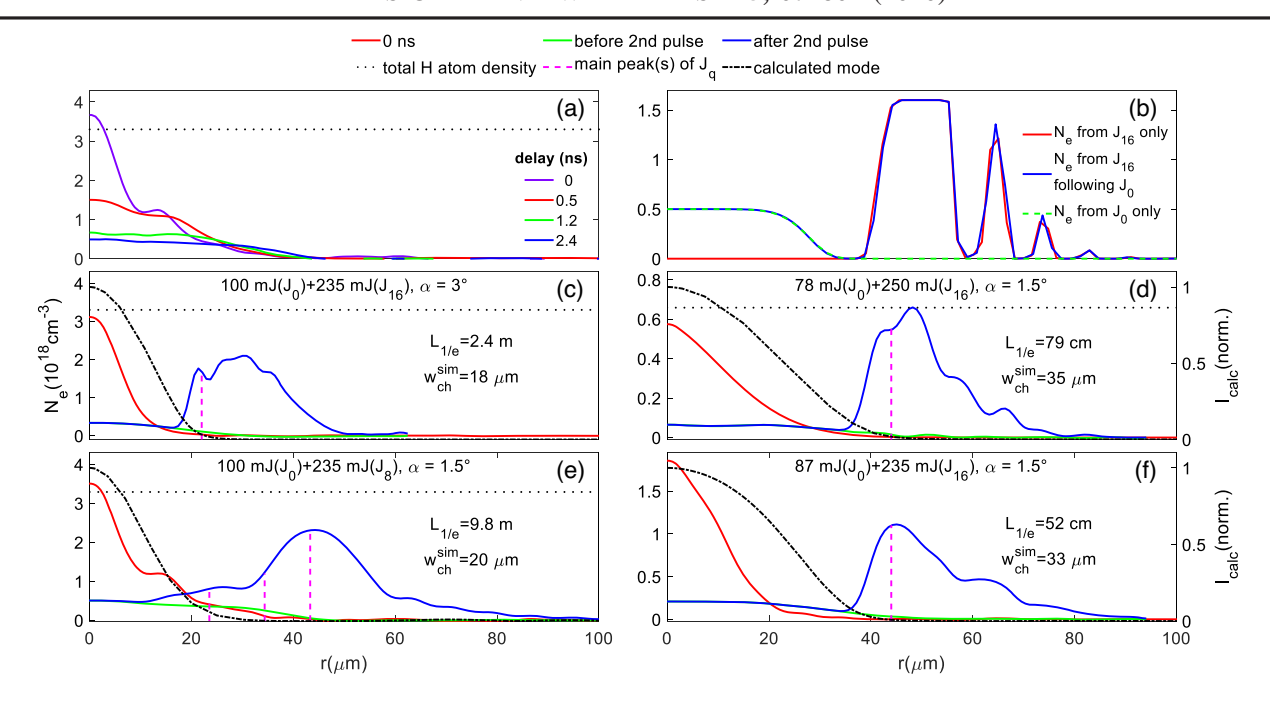


FIG. 4. Transverse electron density profiles in backfill and gas jet hydrogen plasmas. Where shown, the magenta dashed lines indicate maxima of  $J_q$  rings. (a)  $J_0$ -generated core electron density profiles vs time delay. (b)  $J_{16}$  pulse propagation simulations of plasma profile generation with and without  $J_0$ -generated core plasma present.  $\alpha=1.5^\circ$ . (c)–(f) Electron density profiles measured ~10 ps after the  $J_0$  pulse (red curves) and 10 ps before and after the  $J_q$  pulse (green and blue curves). (c) 100 mJ ( $J_0$ ) +235 mJ ( $J_{16}$ ),  $\alpha=3^\circ$ ,  $H_2$  backfill pressure P=50 torr. Waveguide length L=15 cm; (d) 78 mJ ( $J_0$ ) +250 mJ ( $J_{16}$ ),  $\alpha=1.5^\circ$ ,  $H_2$  backfill pressure P=50 torr. Waveguide length L=30 cm; (e) 100 mJ ( $J_0$ ) +235 mJ ( $J_8$ ),  $\alpha=1.5^\circ$ ,  $H_2$  backfill pressure P=50 torr. Waveguide length L=30 cm; (f)  $H_2$  gas jet,  $P\approx30$  torr: 87 mJ ( $J_0$ ) +235 mJ ( $J_{16}$ ),  $\alpha=1.5^\circ$ , q=16. Waveguide length L=5 cm.

index analysis (using  $\Delta N_e \sim 0.75 \times 10^{18} \, \mathrm{cm}^{-3}$ ,  $a \sim 40 \, \mu \mathrm{m}$ , and  $V \sim 2.0$ ) gives  $w_{\mathrm{ch}} \sim 30 \, \mu \mathrm{m}$ , in reasonable agreement with the leaky mode computation.

Guided modes for the L=5–30 cm waveguides of Fig. 4 are shown in Fig. 5, where the modes of Figs. 5(a)–5(d) correspond to the conditions of Figs. 4(c)–4(f) [and Figs. 5(d), 5(e), and 4(f) are for the jet experiment]. For these spot sizes and guide lengths, the number of Rayleigh lengths of guiding (at  $\lambda=800$  nm) ranges over  $L/z_0\sim25$  to  $\sim260$ . In all cases, backfill and gas jet, the guided pulse was injected into the waveguide within  $\sim10$  ps after the cladding-generating  $J_q$  pulse. Even though the core

expands over  $\sim 2$  ns and the cladding collapses in  $\sim 0.5$  ns, as seen in Figs. 2 and 3, this does not limit the length of fixed-parameter waveguides produced using our method: any guided pulse can propagate a couple of nanoseconds behind the  $J_0$  pulse and immediately behind the traveling wave cladding formation by the  $J_q$  pulse. As can be seen in Fig. 5, the guided modes are slightly asymmetric, owing to imperfectly corrected azimuthal intensity variations in the  $J_q$  beam. This leads to slight azimuthal guide variations, as we have determined using a new quasi-2D Abel inversion algorithm employing the measured  $J_q$  beam asymmetry (Supplemental Material [27]). The guided mode radii  $w_{\rm ch}$  in

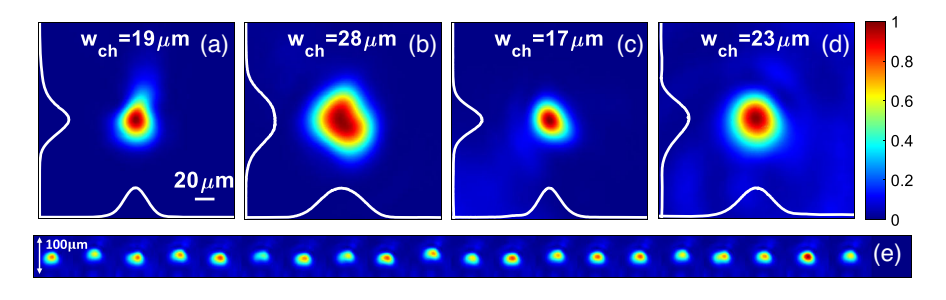


FIG. 5. (a)–(c) Low intensity exit modes from L=15, 30, and 30 cm long plasma waveguides [number of Rayleigh ranges  $L/z_0 \sim 110$ , 100, and 260 (for  $\lambda=800$  nm)] under conditions of Figs. 4(c)–4(e), for injection of  $\sim 100~\mu J$ ,  $\lambda=400$  nm pulse. (d) Gas jet experiment: high intensity exit mode of a 5 cm long waveguide generated in H<sub>2</sub> gas jet. Injected pulse 40 mJ,  $\lambda=800$  nm, 50 fs FWHM, with  $\sim 50\%$  coupling efficiency, giving guided intensity  $\sim 6\times 10^{16}~\mathrm{W/cm^2}$  over  $L/z_0\sim 25$  Rayleigh ranges. (e) Guided modes from 20 successive gas jet shots for conditions of (d). Variations are mainly from injected beam pointing fluctuations.

the figure are from 2D Gaussian fits to the measured mode and agree reasonably well with the computed modes, where the electron density profiles were azimuthally averaged from the extracted 2D profiles.

The guided mode in the hydrogen jet plasma waveguide [Fig. 5(d)] has peak intensity  $\sim 6 \times 10^{16}$  W/cm², based on  $\sim 50\%$  coupling efficiency limited by poor mode matching, owing to injected beam clipping on the axicon hole, and available laser energy limited to 40 mJ. Simulations show that nearly 100% coupling efficiency is possible. There was no evidence of additional ionization by the guided pulse, consistent with our density profile measurements showing fully ionized waveguide cores. Exit modes from a sequence of 20 successive gas jet shots are shown in Fig. 5(e). Pointing fluctuations of the injected pulse are mainly responsible for the variation shown.

Based on the results presented here, we can estimate potential electron acceleration driven by a more powerful laser than ours. As an example, the waveguide in Fig. 4(d) has a core electron density of  $N_{e0} \sim 5 \times 10^{16} \text{ cm}^{-3}$  and  $w_{\rm ch} = 35 \ \mu \rm m$ . This corresponds to a LWFA dephasing length  $L_{\rm deph} \approx 1.3$  m [2,11], which exceeds  $L_{1/e} \sim 0.8$  m for this guide. A resonant pulse with  $a_0 = 1.15$  (for which  $L_{\rm deph} \sim L_{\rm depletion}$ ) and  $\tau \approx (\lambda_p/c)/(\pi\sqrt{2}) \sim 110$  fs guided over  $L_{1/e}$  would give an energy gain  $\Delta E_{\rm accel} \sim 7$  GeV [11] for laser energy 6 J and peak power 55 TW. As seen from the waveguide examples in Fig. 4, wide control over  $w_{\rm ch}$ and  $L_{1/e}$  is possible. Improving the mode confinement so that  $L_{1/e} > L_{\rm deph}$  would give  $\Delta E_{\rm accel} \sim 11$  GeV. Increasing the guided spot size to  $w_{\rm ch} \approx \lambda_p/2 = 75~\mu{\rm m}$  for the same  $N_{e0}$  and extending the corresponding waveguide so that  $L_{1/e} > L_{\text{deph}} \sim 2 \text{ m}$ , would yield  $\Delta E_{\text{accel}} \sim 18 \text{ GeV}$  for laser energy 27 J and peak power 245 TW, with  $\sim$ 5× more charge accelerated. For this case, the laser energy cost for the waveguide would be  $< \sim 5$  J. The ability of these waveguides to guide small spots can lead to even higher energy gain for a given laser energy, but smaller values of  $k_p w_{\rm ch}$  (as in the first example above) are on the edge of the bubble regime [11]; future work will explore whether this is a useful operating condition.

In conclusion, we have presented a new, highly tunable technique for generating long, low loss plasma waveguides for a wide range of plasma densities and guided optical modes. We have demonstrated guiding in waveguides up to 30 cm and over 250 Rayleigh lengths, with a guided intensity limited only by our available laser energy. This technique is ideal for multi-GeV laser wakefield acceleration.

The authors thank M. Tomlinson for technical assistance and A. Picksley, A. Ross, and S. Hooker for useful discussions. This research is supported by the US Department of Energy (DESC0015516) and the National Science Foundation (PHY1619582).

- \*These authors contributed equally to this work.
- T. Tajima and J. M. Dawson, Laser Electron Accelerator, Phys. Rev. Lett. 43, 267 (1979).
- [2] E. Esarey, C. B. Schroeder, and W. P. Leemans, Physics of laser-driven plasma-based electron accelerators, Rev. Mod. Phys. 81, 1229 (2009).
- [3] F. Salehi, A. J. Goers, G. A. Hine, L. Feder, D. Kuk, B. Miao, D. Woodbury, K. Y. Kim, and H. M. Milchberg, MeV electron acceleration at 1 kHz with <10 mJ laser pulses, Opt. Lett. **42**, 215 (2017).
- [4] D. Guénot, D. Gustas, A. Vernier, B. Beaurepaire, F. Böhle, M. Bocoum, M. Lozano, A. Jullien, R. Lopez-Martens et al., Relativistic electron beams driven by kHz single-cycle light pulses, Nat. Photonics 11, 293 (2017).
- [5] F. Albert and A. G. R. Thomas, Applications of laser wakefield accelerator-based light sources, Plasma Phys. Controlled Fusion 58, 103001 (2016).
- [6] 3rd European Advanced Accelerator Concepts Workshop (EAAC2017), edited by U. Dorda, R. Assmann, M. Ferrario, E. Gschwendtner, B. Holzer, A. Mosnier, J. Osterhoff, A. Specka, A. Walker, and R. Walczak, Nuclear Instruments and Methods in Physics Research Section A (2018), Vol. 909, pp. 1–506.
- [7] 2018 IEEE Advanced Accelerator Concepts Workshop (AAC), edited by E. I. Simakov, N. Yampolsky, and K. P. Wootton (IEEE, Breckenridge, CO, 2018).
- [8] W. Lu, C. Huang, M. Zhou, W. B. Mori, and T. Katsouleas, Nonlinear Theory for Relativistic Plasma Wakefields in the Blowout Regime, Phys. Rev. Lett. 96, 165002 (2006).
- [9] W. Lu, M. Tzoufras, C. Joshi, F. S. Tsung, W. B. Mori, J. Vieira, R. A. Fonseca, and L. O. Silva, Generating multi-GeV electron bunches using single stage laser wakefield acceleration in a 3D nonlinear regime, Phys. Rev. ST Accel. Beams 10, 061301 (2007).
- [10] X. Wang, R. Zgadzaj, N. Fazel, Z. Li, S. A. Yi, X. Zhang, W. Henderson, Y. Y. Chang, R. Korzekwa *et al.*, Quasimonoenergetic laser-plasma acceleration of electrons to 2 GeV, Nat. Commun. 4, 1988 (2013).
- [11] C. B. Schroeder, E. Esarey, C. G. R. Geddes, C. Benedetti, and W. P. Leemans, Physics considerations for laser-plasma linear colliders, Phys. Rev. ST Accel. Beams 13, 101301 (2010).
- [12] S. Y. Kalmykov, X. Davoine, I. Ghebregziabher, R. Lehe, A. F. Lifschitz, and B. A. Shadwick, Controlled generation of comb-like electron beams in plasma channels for polychromatic inverse Thomson γ-ray sources, Plasma Phys. Controlled Fusion 58, 034006 (2016).
- [13] C. G. Durfee and H. M. Milchberg, Light Pipe for High Intensity Laser Pulses, Phys. Rev. Lett. **71**, 2409 (1993).
- [14] V. Kumarappan, K. Y. Kim, and H. M. Milchberg, Guiding of Intense Laser Pulses in Plasma Waveguides Produced from Efficient, Femtosecond End-Pumped Heating of Clustered Gases, Phys. Rev. Lett. 94, 205004 (2005).
- [15] N. Lemos, T. Grismayer, L. Cardoso, G. Figueira, R. Issac, D. A. Jaroszynski, and J. M. Dias, Plasma expansion into a waveguide created by a linearly polarized femtosecond laser pulse, Phys. Plasmas 20, 063102 (2013).
- [16] R. J. Shalloo, C. Arran, L. Corner, J. Holloway, J. Jonnerby, R. Walczak, H. M. Milchberg, and S. M. Hooker, Hydrodynamic optical-field-ionized plasma channels, Phys. Rev. E 97, 053203 (2018).

- [17] N. Lemos, L. Cardoso, J. Geada, G. Figueira, F. Albert, and J. M. Dias, Guiding of laser pulses in plasma waveguides created by linearly-polarized femtosecond laser pulses, Sci. Rep. 8, 3165 (2018).
- [18] R. J. Shalloo, C. Arran, A. Picksley, A. von Boetticher, L. Corner, J. Holloway, G. Hine, J. Jonnerby, H. M. Milchberg, C. Thornton, R. Walczak, and S. M. Hooker, Low-density hydrodynamic optical-field-ionized plasma channels generated with an axicon lens, Phys. Rev. Accel. Beams 22, 041302 (2019).
- [19] T. R. Clark and H. M. Milchberg, Optical mode structure of the plasma waveguide, Phys. Rev. E **61**, 1954 (2000).
- [20] C. G. Durfee, J. Lynch, and H. M. Milchberg, Development of a plasma waveguide for high-intensity laser pulses, Phys. Rev. E 51, 2368 (1995).
- [21] T. M. Antonsen, Jr. and P. Mora, Leaky Channel Stabilization of Intense Laser Pulses in Tenuous Plasmas, Phys. Rev. Lett. 74, 4440 (1995).
- [22] Y. Ehrlich, C. Cohen, A. Zigler, J. Krall, P. Sprangle, and E. Esarey, Guiding of High Intensity Laser Pulses in Straight and Curved Plasma Channel Experiments, Phys. Rev. Lett. 77, 4186 (1996).
- [23] A. Butler, D. J. Spence, and S. M. Hooker, Guiding of High-Intensity Laser Pulses with a Hydrogen-Filled Capillary Discharge Waveguide, Phys. Rev. Lett. 89, 185003 (2002).
- [24] A. J. Gonsalves, K. Nakamura, J. Daniels, C. Benedetti, C. Pieronek, T. C. H. de Raadt, S. Steinke, J. H. Bin, S. S. Bulanov *et al.*, Petawatt Laser Guiding and Electron Beam Acceleration to 8 GeV in a Laser-Heated Capillary Discharge Waveguide, Phys. Rev. Lett. 122, 084801 (2019).
- [25] A. J. Gonsalves, F. Liu, N. A. Bobrova, P. V. Sasorov, C. Pieronek, J. Daniels, S. Antipov, J. E. Butler, S. S. Bulanov, W. L. Waldron, D. E. Mittelberger, and W. P. Leemans, Demonstration of a high repetition rate capillary discharge waveguide, J. Appl. Phys. 119, 033302 (2016).
- [26] P. B. Corkum, N. H. Burnett, and F. Brunel, Above-Threshold Ionization in the Long-Wavelength Limit, Phys. Rev. Lett. 62, 1259 (1989).
- [27] See Supplemental Material at http://link.aps.org/supplemental/ 10.1103/PhysRevLett.125.074801 for quasi-2D Abel inversion, calculation of quasi-bound modes and leakage, and simulation of ultrashort Bessel beam pulse propagation and ionization, which includes Refs. [28–34].
- [28] M. Takeda, H. Ina, and S. Kobayashi, Fourier-transform method of fringe-pattern analysis for computer-based topography and interferometry, J. Opt. Soc. Am. 72, 156 (1982).

- [29] V. Dribinski, A. Ossadtchi, V. A. Mandelshtam, and H. Reisler, Reconstruction of Abel-transformable images: The Gaussian basis-set expansion Abel transform method, Rev. Sci. Instrum. 73, 2634 (2002).
- [30] K. Okamoto, Fundamentals of Optical Waveguides (Academic Press, New York, 2005).
- [31] M. Kolesik and J. V. Moloney, Nonlinear optical pulse propagation simulation: From Maxwell's to unidirectional equations, Phys. Rev. E **70**, 036604 (2004).
- [32] V. S. Popov, Tunnel and multiphoton ionization of atoms and ions in a strong laser field (Keldysh theory), Phys. Usp. 47, 855 (2004).
- [33] S. V. Popruzhenko, V. D. Mur, V. S. Popov, and D. Bauer, Strong Field Ionization Rate for Arbitrary Laser Frequencies, Phys. Rev. Lett. 101, 193003 (2008).
- [34] J. K. Wahlstrand, S. Zahedpour, Y.-H. Cheng, J. P. Palastro, and H. M. Milchberg, Absolute measurement of the ultrafast nonlinear electronic and rovibrational response in H<sub>2</sub> and D<sub>2</sub>, Phys. Rev. A **92**, 063828 (2015).
- [35] I. Pagano, J. Brooks, A. Bernstein, R. Zgadzaj, J. Leddy, J. Cary, and M. C. Downer, Low Density Plasma Waveguides Driven by Ultrashort (30 fs) and Long (300 ps) Pulses for Laser Wakefield Acceleration, *IEEE Advanced Accelerator Concepts Workshop (AAC)* (IEEE, Breckenridge, 2018).
- [36] Bo Miao et al. (to be published).
- [37] J. Fan, E. Parra, I. Alexeev, K. Y. Kim, H. M. Milchberg, L. Y. Margolin, and L. N. Pyatnitskii, Tubular plasma generation with a high-power hollow Bessel beam, Phys. Rev. E 62, R7603 (2000).
- [38] W. D. Kimura, H. M. Milchberg, P. Muggli, X. Li, and W. B. Mori, Hollow plasma channel for positron plasma wakefield acceleration, Phys. Rev. ST Accel. Beams 14, 041301 (2011).
- [39] S. Gessner, E. Adli, J. M. Allen, W. An, C. I. Clarke, C. E. Clayton, S. Corde, J. P. Delahaye, J. Frederico *et al.*, Demonstration of a positron beam-driven hollow channel plasma wakefield accelerator, Nat. Commun. 7, 11785 (2016).
- [40] T. R. Clark and H. M. Milchberg, Time- and Space-Resolved Density Evolution of the Plasma Waveguide, Phys. Rev. Lett. 78, 2373 (1997).
- [41] D. Marcuse, Loss analysis of single-mode fiber splices, Bell Syst. Tech. J. **56**, 703 (1977).
- [42] JE. Shrock et al. (to be published).